

# Physical processes in the X-ray/gamma-ray source of IC 4329A

A. A. Zdziarski,<sup>1</sup>★ A. C. Fabian,<sup>2</sup> K. Nandra,<sup>2</sup> A. Celotti,<sup>2</sup> M. J. Rees,<sup>2</sup> C. Done,<sup>3</sup>  
P. S. Coppi<sup>4</sup> and G. M. Madejski<sup>5</sup>†

<sup>1</sup>*N. Copernicus Astronomical Center, Bartycka 18, 00-716 Warsaw, Poland*

<sup>2</sup>*Institute of Astronomy, Madingley Road, Cambridge CB3 0HA*

<sup>3</sup>*Physics Department, Leicester University, Leicester LE1 7RH*

<sup>4</sup>*Department of Astronomy and Astrophysics, University of Chicago, 5640 Ellis Avenue, Chicago, IL 60637, USA*

<sup>5</sup>*Laboratory for High Energy Astrophysics, NASA/Goddard Space Flight Center, Greenbelt, MD 20771, USA*

Accepted 1994 June 16. Received 1994 May 17

## ABSTRACT

Theoretical implications of the recent simultaneous *ROSAT*/OSSE observation of the Seyfert 1 IC 4329A are discussed. We find that either thermal or non-thermal Comptonization models can fit the data. Thermal models require optically thin plasma and mildly relativistic electrons. Non-thermal models require most of the injected power to be at low values of the electron Lorentz factor. Both models predict a spectral cut-off at energies below  $\sim 1$  MeV, which agrees with broad-band data including non-simultaneous *Ginga* spectra that match the *ROSAT* 2-keV flux. Also, Compton reflection corresponding to cold matter covering a solid angle of  $2\pi$  is required, and partial covering is ruled out.

Since the spectrum of IC 4329A is typical of Seyfert 1s, their contribution to the cosmic hard X-ray background can be estimated: without cosmological evolution, it is 30 per cent at 3 keV. As the peak of the  $\nu F_\nu$  spectrum of IC 4329A is much broader than that of the hard X-ray background, however, Seyfert 1s cannot account for the X-ray background spectrum without spectral evolution.

**Key words:** galaxies: individual: IC 4329A – galaxies: Seyfert – diffuse radiation – X-rays: galaxies.

## 1 INTRODUCTION

In this paper, we discuss theoretical implications of the simultaneous observation of the Seyfert 1 IC 4329A by *ROSAT* and OSSE aboard the *GRO* (Madejski et al. 1994, hereafter M94). The data given in M94 are well fitted by an intrinsic power law with an exponential cut-off, external absorption and a Compton reflection component [using the angle-averaged formula of Lightman & White (1988) and White, Lightman & Zdziarski (1988)]. The best-fitting parameters are a power-law energy index of  $\alpha = 0.87^{+0.21}_{-0.07}$ , a cut-off energy of  $E_C = 220^{+100}_{-110}$  keV, and a (poorly constrained) relative normalization of the reflected component ( $f_r$ ) of about unity (model A in M94). An exponential cut-off is not required by the *ROSAT*/OSSE data; only the upper limit from EGRET on the *GRO* implies that  $E_C \lesssim 300$  MeV. The model with  $E_C = 300$  MeV has  $\alpha = 1.07$  and  $f_r = 2$ .

The spectral constraints become much tighter with the inclusion of archival *Ginga* data. Although these are not simultaneous, they match the flux measured by *ROSAT* at 2 keV. The best fits to two sets of *Ginga* observations give  $0.92 < \alpha < 1$ ,  $250 < E_C < 1700$  keV, and  $0.9 < f_r < 1.4$  (models B and C in M94). As the X-ray spectral *shape* in IC 4329A is fairly constant (Fiore et al. 1992), these parameters indeed give a plausible broad-band spectrum of the active galactic nucleus (AGN). Furthermore, M94 find that the OSSE spectrum also remains constant with time, which allows them to use the spectrum from the sum of this and two previous OSSE observations. This reduces the allowed range of  $E_C$  to between 240 and 900 keV. We note that this value of  $E_C$  is much larger than that seen in the brightest Seyfert, NGC 4151 (Maisack et al. 1993; Zdziarski, Lightman & Maciołek-Niedźwiecki 1993).

The X-ray/ $\gamma$ -ray spectrum of IC 4329A is very typical for Seyfert 1s. Its intrinsic X-ray spectral index is consistent with the average one for Seyferts,  $\alpha = 0.95 \pm 0.05$  (Pounds et al. 1990; Nandra & Pounds 1994, hereafter NP94), and the

★ E-mail: aaz@camk.edu.pl

† Universities Space Research Association.

relative normalization of the reflection component is close to the average Seyfert value ( $f_r \approx 1.0 \pm 0.2$ , NP94; note that we have multiplied their normalization, corresponding to the face-on reflection spectrum, by 1.33 in order to get  $f_r$  for the angle-averaged reflection spectrum; see Ghisellini, Haardt & Matt 1994). The  $\gamma$ -ray spectral index in the OSSE range (50–200 keV),  $\alpha = 1.6 \pm 0.2$ , is again very similar to the average index for Seyferts observed by OSSE,  $\alpha = 1.4 \pm 0.25$  (Johnson et al. 1994). Thus, unlike NGC 4151, conclusions regarding the nature of the X-ray/ $\gamma$ -ray source in IC 4329A are likely to be applicable to Seyfert 1s as a class. In particular, the contribution of Seyfert 1s to the cosmic X-ray background (hereafter XRB) can be re-evaluated using the spectrum of IC 4329A.

## 2 MODELS OF THE X-RAY/ $\gamma$ -RAY SOURCE

### 2.1 Thermal Compton scattering

Optically thin thermal Compton scattering spectra are well represented by power laws with exponential cut-offs (e.g. Zdziarski 1986). This spectral form was in fact used to fit the data (section 1, M94). An intrinsic spectrum with  $\alpha = 0.95$  and  $E_C = 400$  keV (within the confidence regions of models D and E in M94) is almost identical to the thermal Comptonization spectrum (obtained using the Monte Carlo method of Górecki & Wilczewski 1984) from a slab irradiated from below by UV photons with  $kT = 256$  keV ( $E_C \approx 1.6kT$ ) and  $\tau = 0.09$ , as shown in Fig. 1. The scattering plasma has to be *optically thin* in general, since the allowed range of  $\alpha \approx 1$  and  $E_C$  ( $> 110$  keV, using the *ROSAT*/OSSE data only: M94) implies  $\tau \lesssim 0.5$  [see equations (1) and (2) below]. Compton scattering in optically thick plasmas (Sunyaev & Titarchuk 1980) is ruled out.

Quantitatively, for optically thin plasmas we have

$$\alpha \approx \frac{-\ln P}{\ln(1 + 4\Theta + 16\Theta^2)} \quad (1)$$

(Zdziarski 1985, hereafter Z85; Pozdnyakov, Sobol' & Sunyaev 1977), where  $\Theta \equiv kT/m_e c^2$ ,  $m_e$  being the electron rest mass, and  $P$  is the average scattering probability, which for a uniform slab is

$$P = 1 + \frac{\exp(-\tau)}{2} \left( \frac{1}{\tau} - 1 \right) - \frac{1}{2\tau} + \frac{\tau}{2} E_1(\tau) \\ \rightarrow \begin{cases} -(\tau/2) \ln \tau, & \tau \ll 1; \\ 1 - 1/(2\tau), & \tau \gg 1, \end{cases} \quad (2)$$

where  $E_1$  is the exponential integral (Press et al. 1992). Equations (1) and (2) fit Monte Carlo results well for any  $T$ , for  $\tau \lesssim$  a few.

Furthermore, Monte Carlo simulations show that spectra for  $\Theta \geq 1$  (which correspond to  $\tau \lesssim 0.02$  and  $E_C \geq 800$  keV) are very bumpy, with distinct individual scattering profiles (see e.g. Haardt & Maraschi 1993, hereafter HM93). Since the intrinsic X-ray power law in IC 4329A is smooth,  $E_C \lesssim 800$  keV is required, which approximately agrees with the fitted maximum  $E_C$  (models D and E of M94) (unless a spatial distribution of plasma parameters is fine-tuned to give a smooth  $\alpha \approx 1$  power law over the 1–30 keV range).

The parameters for the thermal Comptonization model in Fig. 1 are consistent with the disc-corona model of HM93 with most of the accretion power released in the corona. This is because, in our Monte Carlo model, the seed photon power equals almost exactly the power in the photons scattered back towards the slab (crosses in Fig. 1) and thermal-

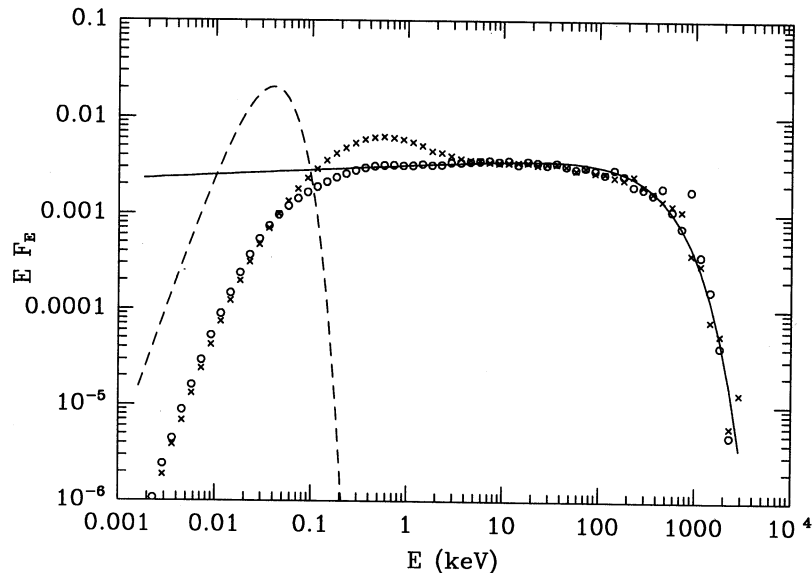


**Figure 1.** An optically thin thermal Comptonization model for the intrinsic spectrum of IC 4329A. Blackbody photons (dashed curve;  $kT_{\text{bb}} = 10$  eV) emitted by a disc are Compton-upscattered in a thermal corona with  $kT = 256$  keV and  $\tau = 0.09$ . Circles and crosses give the spectra of photons emitted away from and of photons scattered back to the disc, respectively. The powers in those spectra are 1.0 and 1.25, respectively, of the power in the seed photons. Note that the total emitted spectrum also includes unscattered blackbody photons (not shown here). The solid curve, which gives the intrinsic spectrum of IC 4329A [ $\propto E^{1-\alpha} \exp(-E/E_C)$ ,  $\alpha = 0.95$ ,  $E_C = 400$  keV], approximates well the emitted spectrum. As  $\sim 80$  per cent of the power in photons scattered back to the disc is absorbed and thermalized ( $\sim 20$  per cent is reflected by the cold disc, the component of which is not shown here), all the blackbody emission is due to the absorbed power and very little internal dissipation in the disc is allowed. Thus, this model fits well the dissipative corona-disc scenario of HM93.

ized. This then implies that all the disc thermal emission is due to reprocessing of the hard X-ray flux, and that the intrinsic, thermal viscous stress emission from the disc is negligible. Models with  $E_C \lesssim 400$  keV require larger values of  $\tau$  in order to produce the observed  $\alpha$ . For the same incident blackbody flux, the scattered spectrum (which starts at a point a factor of  $\sim \tau$  below the peak flux of the blackbody) is then higher in normalization. Thus this model predicts rather more reprocessed blackbody flux than for  $E_C = 400$  keV, and so is not consistent with the disc-corona model. This problem can be circumvented, however, if a fraction of the reprocessed photons do not return to the hot scattering cloud (which can be achieved if the hot cloud is at some height above the disc). On the other hand, models with  $E_C \gtrsim 400$  keV allow for some dissipation taking place in the disc.

Is the X-ray/ $\gamma$ -ray source made of electrons or of pairs? As the plasma is optically thin, the answer depends sensitively on the pair escape rate (Z85). In the absence of that process, the ‘standard’ pair equilibrium (e.g. Svensson 1984) applies, with the pair production rate (dominated by photon-photon interactions) balanced by pair annihilation in the hot cloud. The plasma is pair-dominated for the maximum allowed (local) compactness,  $\ell_1 \sim 20$  for  $E_C = 400$  keV, which decreases (increases) quickly with increasing (decreasing)  $E_C$  (see fig. 3b of HM93). The annihilation feature is, however, broad and not distinguishable from the continuum (Zdziarski 1986). For  $\ell_1$  much lower than the maximum  $\ell_1(E_C)$ , the plasma is  $e^-$ -dominated. Furthermore, in the corona geometry we have to distinguish the local compactness, i.e. that corresponding to the luminosity  $L$  produced locally in a volume with size equal to the corona scaleheight  $H$ , from the global compactness,  $\ell \equiv L\sigma_T/(Rm_e c^3) \approx (3R/H)\ell_1$ , where  $R$  is the corona radius (Björnsson & Svensson 1991) and  $\sigma_T$  is the Thomson cross-section. In gas-pressure-dominated  $e^-$  coronae,  $H/R \approx 0.03r^{1/2}$ , where  $r \equiv R/R_S$  (Svensson & Zdziarski 1994), and thus  $\ell \approx 100r^{-1/2}\ell_1$ . ( $R_S$  is the Schwarzschild radius.) From the observed iron linewidth,  $r < 50$  (Done, in preparation), and thus the corona would be  $e^-$ -dominated for  $\ell \ll 300$  (at  $E_C = 400$  keV).

However, pair escape can cause the corona to be  $e^-$ -dominated even at much larger  $\ell$ . Pairs can diffuse to the disc with an effective pair velocity  $\beta$  and annihilate there or be blown away by the radiation pressure. (Note that an annihilation line from escaping pairs is negligibly weak, with the local compactness in the annihilation photons of  $< \beta\tau \ll 1$ .) The ratio of this process to the coronal annihilation is  $\sim 20\beta/\tau \sim 200\beta$  (at  $\Theta = 0.5$ ; Z85). The compactness at which the corona can be pair-dominated increases then by the same factor, and the condition for the  $e^-$ -domination in the paragraph above becomes  $\ell \ll 6 \times 10^4 \beta$ . Since  $\ell < 10^3$  is expected in sub-Eddington accretion sources (Svensson 1987, hereafter S87), any  $\beta \gtrsim 0.02$  (i.e. even much below the sound speed) would cause the corona to be  $e^-$ -dominated. In conclusion, the corona in IC 4329A is likely to consist of electrons unless pair escape to both the disc and the exterior is strongly suppressed.

## 2.2 Non-thermal plasmas

As discussed in Section 1, a spectral break in the intrinsic (power law) spectrum is *not* required if one takes into

account only the simultaneous *ROSAT*/*OSSE* data. A single power-law spectrum extending to  $\gamma$ -rays can be naturally produced by non-thermal power-law electrons with a power-law index of  $p = 2\alpha + 1 \approx 3$  (e.g. Blumenthal & Gould 1970). The power-law electrons can scatter, for example, UV photons emitted by an accretion disc. If this is the case, the power-law distribution has to continue down to Lorentz factors  $\gamma \sim 3$ , for the upscattering of the UV photons (with characteristic energy of  $\sim 50$  eV or so) to form a power law with  $\alpha \approx 1$  above 0.7 keV, as required by the data (M94). Also, the compactness of the non-thermal source has to be low,  $\ell_{\text{nth}} \lesssim 1$ , for pair production not to modify the power-law spectrum (e.g. S87; Lightman & Zdziarski 1987). In this limit, pair absorption cuts off the spectrum above  $E_C \sim 150$  MeV/ $\ell$  (S87).

The compactness in accreting black hole sources, however, is likely to be  $\gtrsim 1$  (S87), and then the pair production effects dominate. The energetic electrons cool before they can escape, so their distribution is described by the continuity equation where the injected spectrum is balanced against Compton cooling. For injected distributions of the form  $\gamma^{-s}$ ,  $s < 1$  gives  $p = 2$ , while, for  $s \geq 1$ ,  $p = s + 1$ . ‘Standard’ non-thermal pair models use monoenergetic injection of pairs or electrons, which Compton-cool on the UV photons to produce a power-law particle distribution of  $p = 2$  (e.g. S87). Thus for  $\ell_{\text{nth}} \ll 1$  the spectrum has  $\alpha = 0.5$ . An increase of  $\ell_{\text{nth}}$  increases the amount of pair reprocessing if  $\gamma$ -rays are produced, i.e. for large particle Lorentz factors. This increases the spectral index to  $\alpha \sim 1$ , but also increases the number of cooled pairs in the source. This gives rise to a pair annihilation line containing about 10 per cent (the pair yield) of the injected power. Downscattering of the line superimposed on the non-thermal emission and the reflection component causes the spectrum above  $\sim 200$  keV to be *above* the observational upper limits. The best monoenergetic injection pair model by Lightman & Zdziarski (1987, fitted to the same data set as in model D of M94) has  $\ell_{\text{nth}} = 70$  with injection at  $\gamma_i = 6000^{+4000}_{-1500}$ , a compactness corresponding to the seed blackbody photons (at  $kT_{\text{bb}} = 10$  eV),  $\ell_{\text{bb}} = 600$ , and a reflection normalization  $f_r = 1.0$ . The model yields  $\Delta\chi^2 = 25$  with respect to the best-fitting thermal model (D in M94); this increase is due mostly to the photon flux in the 180–360 keV range being  $4\sigma$  above the *OSSE* sensitivity. The fit can be only slightly improved if one allows for pair escape (either diffusion to the disc or pair wind, see Section 2.1), since this gives fewer cooled pairs and a weaker annihilation feature. For the effective escape velocity  $\beta = 0.3$ ,  $\Delta\chi^2 = 17$ , which still allows us to rule out the monoenergetic injection non-thermal model.

On the other hand, non-thermal models with substantial power supplied to the source at moderately relativistic energies have lower pair yield and can fit the data. One example is a model with a steep power-law injection (which gives a steep intrinsic spectrum, producing fewer secondary pairs). The best-fitting model (Lightman & Zdziarski 1987; fitted to the same data set as in model E of M94) is shown in Fig. 2. It yields the same  $\chi^2$  as the best-fitting thermal model. Still, the model predicts the photon flux in the 180–360 keV range at  $2.8\sigma$  above the *OSSE* sensitivity. Since this sensitivity can be increased by increasing the detection time, this model can be tested in the near future.

As noted by, for example, Ghisellini, Haardt & Fabian (1993), electron injection at  $\gamma_i \gtrsim 5$  gives rise to spectra

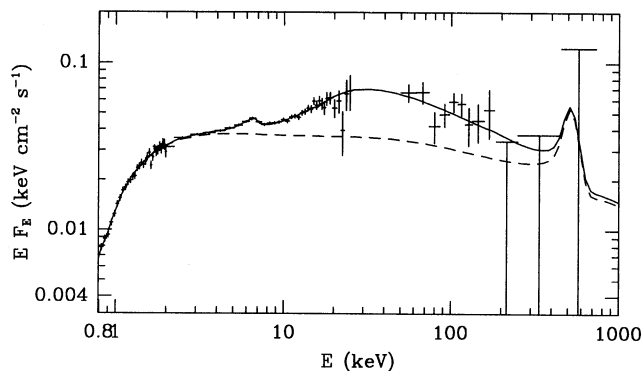


**Figure 2.** A fit of a non-thermal model with  $e^\pm$  pair production and a power-law pair injection to the broad-band spectrum of IC 4329A (from *ROSAT*, *Ginga* and OSSE; the upper limits are  $2\sigma$ ). The dashed curve gives the non-thermal pair emission alone, and the solid curve is the sum of the pair emission and a Compton reflection component (with an iron  $K\alpha$  line). The parameters are  $s=2.8$ ,  $\ell_{\text{nth}}=70$ ,  $\gamma_{\text{min}}=5$ ,  $\gamma_{\text{max}}=10^3$  (fixed),  $\ell_{\text{bb}}=30$  and  $f_r=1.50$ .

extending only slightly above the threshold for pair production, which results in very few pairs. The spectra in this model are from repeated Compton scattering by non-thermal electrons, and are very similar to those from thermal Compton scattering. We have tested this model using the code by Coppi (1992), and have obtained a good fit ( $\alpha \approx 1$  and a strong cut-off above  $\sim 300$  keV) for  $\ell_{\text{nth}}=70$ ,  $\ell_{\text{bb}}=20$ , and monoenergetic electron injection at  $\gamma_i=3.5$ .

### 2.3 The presence and state of the reflecting medium

Can the spectrum of IC 4329A be explained by partial covering rather than by reflection? The *continuum* spectral signature of reflection is quite similar to that of partial covering by a substantial column density ( $\sim 10^{24}$  cm $^{-2}$ ) of cold material (Piro, Yamauchi & Matsuoka 1990). The absorbed spectrum only contributes above  $\sim 10$  keV, so the sum of it and the direct component produces a high-energy excess. Note that this is very different from the partial covering considered by M94, in which a much lower  $N_{\text{H}}$  ( $\sim 5 \times 10^{21}$  cm $^{-2}$ ) was used to account for the observed excess below 0.7 keV. However, partial covering, unlike reflection, has the same shape at high energies as the incident spectrum, so a break at an energy lower than in the reflection model is required, as reflection no longer contributes to the steepening in the OSSE band. An incident power-law spectrum without a break or cut-off is now ruled out at higher significance than in the case of reflection [ $\chi^2=172/127$  degrees of freedom (d.o.f.), fitted to the data as in model D of M94]. The intrinsic steepening in the *ROSAT/Ginga/OSSE* data can be modelled either by an exponential cut-off power-law spectrum ( $\alpha=0.85 \pm 0.03$ ,  $E_{\text{C}}=170^{+60}_{-40}$  keV,  $N_{\text{H}}=(2.4 \pm 0.7) \times 10^{24}$  cm $^{-2}$  and covering fraction  $0.29 \pm 0.05$ ;  $\chi^2=105/124$  d.o.f.) or by a broken power law ( $\alpha_1=0.88 \pm 0.02$ ,  $\alpha_2=2.7 \pm 0.3$ ,  $E_{\text{break}}=55 \pm 19$  keV;  $\chi^2=109/123$  d.o.f.) with similar partial covering parameters.

It is difficult, however, to reproduce the observed line emission from such models. For the fitted partial covering, the line equivalent width would be only  $\sim 30$  eV (Inoue 1989), whereas the observed equivalent width is about 110

eV (M94), which agrees with the reflection model (George & Fabian 1991). External sources of the line may be important (Ghisellini et al. 1994) but, in that case, a line much narrower than observed ( $\sigma_{\text{Fe}} \sim 0.5$  keV; Done, in preparation) would be produced. Thus we can rule out partial covering as a model for the overall X-ray/ $\gamma$ -ray spectrum.

The reflecting medium is likely to be partially ionized by the incident photons. We have fitted ionized reflection spectra (Done et al. 1992) to the *ROSAT/Ginga* spectra, and found that  $\xi=L/n_e R^2 \lesssim 50$ , where  $L$  is defined as the total ionizing luminosity between 5 eV and 300 keV, and  $n_e$  is the electron number density. Over the more usual bandpass of 13.6 eV–13.6 keV, this corresponds to  $\xi \lesssim 30$ , where iron is less ionized than Fe xv. This is rather less than the ionization required to produce the observed soft X-ray excesses in some Seyferts from reflection alone (Czerny & Życki 1994).

### 3 CONTRIBUTION TO THE X-RAY/ $\gamma$ -RAY BACKGROUND

As discussed in Section 1, the spectrum of IC 4329A is typical of Seyfert 1s. We thus use it to estimate the contribution of Seyfert 1s to the XRB. The volume emissivity at  $z=0$  from local sources is estimated to be  $\sim 10^{39} h$  erg s $^{-1}$  Mpc $^{-3}$  [ $h \equiv H_0/(100 \text{ km s}^{-1} \text{ Mpc}^{-1})$ ] in the 2–10 keV range (Lahav et al. 1993), which is in fact the same as the estimated local AGN emissivity, dominated by Seyferts (Piccinotti et al. 1982). The solid curve in Fig. 3 shows the contribution to the XRB assuming the best-fitting spectrum of IC 4329A (model D in M94) and no evolution up to  $z_{\text{max}}=5$ . The Seyfert 1 contribution to the XRB is then about 30 per cent at 3 keV and 18 per cent at 340 keV.

On the other hand, Seyfert 1s may undergo evolution of the comoving volume emissivity. We find it has to be slower than  $(1+z)^\beta$ ,  $\beta \approx 1.6$  (with no spectral evolution and a cosmological density parameter  $\Omega_0=0$ ), as the case with  $\beta=1.6$  already produces most of the 2-keV XRB (dotted curve in Fig. 3). The integrated Seyfert 1 spectrum, however, peaks at too low an energy (20 keV) and is much too soft at low energies to explain the XRB peak at 30 keV. This is just a manifestation of the well-known spectral paradox (Boldt 1987) of the striking difference between the spectra of the XRB and of observed AGNs. To reproduce the hard XRB, either suitable *spectral* evolution or a new class of source is required.

It turns out that the contribution of Seyfert 1s to the background cannot constrain the exponential cut-off energy in the spectra of individual Seyfert 1s. The dashed curve in Fig. 3 shows the source model with  $\alpha=1.07$  and a high  $E_{\text{C}}=300$  MeV (see Section 1), and without evolution. We see that this contribution is entirely within the measured  $\gamma$ -ray background. This conclusion differs from that of Rothschild et al. (1983), who required a break in the Seyfert 1 spectrum based on the contribution to the  $\gamma$ -ray background. The difference is due to their average Seyfert 1 spectrum having  $\alpha=0.7$ , whereas *Ginga* showed the intrinsic Seyfert 1 power-law index to be  $\alpha \approx 1$  (NP94).

### 4 CONCLUSIONS

The simplest description of the spectrum of IC 4329A is in terms of thermal Comptonization. In this model, the scatter-

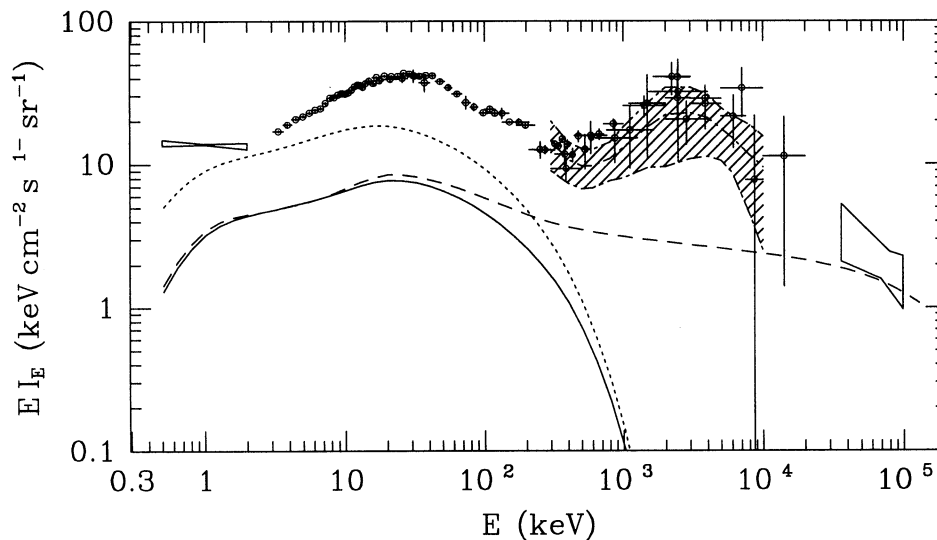


**Figure 3.** The possible contributions of Seyfert 1 galaxies with IC 4329A-like spectra to the cosmic X-ray/ $\gamma$ -ray background. The 0.5–2 keV error contour gives the preliminary *ROSAT* results (Hasinger 1992); circles are a compilation of best results from various experiments by Gruber (1992); the hatched region is the systematic error contour for the *Apollo* results, with the middle dot-dashed curve being the best estimate of the spectrum (Trombka et al. 1977); and the 35–100 MeV error contour is from Fichtel, Simpson & Thompson (1978). The models are for  $\Omega_0 = 0$ , and the 2–10 keV local emissivity of  $10^{39} \text{ h erg s}^{-1} \text{ Mpc}^{-3}$ . The solid and dashed curves give the case without evolution for  $z_{\text{max}} = 5$  and for  $(\alpha = 0.93, E_C = 320 \text{ keV}, f_r = 1.04)$  and  $(\alpha = 1.07, E_C = 300 \text{ MeV}, f_r = 2)$  (M94), respectively. The dotted curve corresponds to the fastest allowed evolution ( $\beta = 1.6, z_{\text{max}} = 4$ ) for the model with  $E_C = 320 \text{ keV}$ .

ing medium has to be *optically thin*, with the Thomson optical depth  $0.02 \lesssim \tau \lesssim 0.5$ , and mildly relativistic,  $100 \lesssim kT \lesssim 500 \text{ keV}$ . Optically thick Comptonization (Sunyaev & Titarchuk 1980) is ruled out. The best-fitting parameters,  $\tau \approx 0.1$  and  $kT \approx 250 \text{ keV}$ , fit well the dissipative disc-corona model of HM93. The plasma in the corona is probably electron-dominated.

The spectrum can also be fitted by non-thermal models, with either power-law electron injection extending to  $\gamma \ll 10$  (and pair production), or monoenergetic injection at  $\gamma_i \sim 3$ , for which very few pairs are produced. Non-thermal pair models with monoenergetic injection (at  $\gamma_i \gg 10$ ) and pair production are ruled out, as they strongly over-predict the flux above 180 keV. This excess flux is partly due to Compton downscattering of the annihilation line.

Both classes of models require a substantial contribution from Compton reflection, and partial covering by optically thick matter is ruled out. The high-energy tail of reflection is important in the OSSE range, resulting in the incident spectrum being harder than the observed one. Therefore the break energy in the incident spectrum is at a much larger energy ( $\sim 500 \text{ keV}$ ) than the break in the observed spectrum (at  $\sim 30 \text{ keV}$ ). Since the spectrum of IC 4329A is very typical of Seyfert 1s, this conclusion is likely to apply to the average Seyfert 1 spectrum, for which a break at  $\sim 50 \text{ keV}$  was inferred based on models *without* reflection (Johnson et al. 1994).

The contribution of Seyfert 1s to the hard XRB, based on the IC 4329A spectrum, is about 20–30 per cent without evolution. The contribution fits neither the 3–10 keV slope nor the 30-keV peak in the background. To fit the XRB, spectral evolution or a different class of object is required.

## ACKNOWLEDGMENTS

This research has been supported in part by NASA grants NAG5 1813, 830, 1284, 1636, 2439, NAGW 3129, Polish KBN grant 221129102 (AAZ) and a *GRO* Fellowship (PSC).

## REFERENCES

- Blumenthal G. R., Gould R. J., 1970, *Rev. Mod. Phys.*, 42, 237
- Björnsson G., Svensson R., 1991, *ApJ*, 371, L69
- Boldt E., 1987, *Phys. Rep.*, 146, 215
- Coppi P. S., 1992, *MNRAS*, 258, 657
- Czerny B., Życki P. T., 1994, *ApJ*, in press
- Done C., Mulchaey J. S., Mushotzky R. F., Arnaud K. A., 1992, *ApJ*, 395, 275
- Fichtel C. E., Simpson G. A., Thompson D. J., 1978, *ApJ*, 222, 833
- Fiore F., Perola G. C., Matsuoka M., Yamauchi M., Piro L., 1992, *A&A*, 262, 37
- George I. M., Fabian A. C., 1991, *MNRAS*, 249, 352
- Ghisellini G., Haardt F., Fabian A. C., 1993, *MNRAS*, 263, L9
- Ghisellini G., Haardt F., Matt G., 1994, *MNRAS*, 267, 743
- Górecki A., Wilczewski W., 1984, *Acta Astron.*, 34, 141
- Gruber D. E., 1992, in Barcons X., Fabian A. C., eds, *The X-Ray Background*. Cambridge Univ. Press, Cambridge, p. 44
- Haardt F., Maraschi L., 1993, *ApJ*, 413, 507 (HM93)
- Hasinger G., 1992, in *ESA Int. Space Year*, 111
- Inoue H., 1989, in Hunt J., Battrick B., eds, *23rd ESLAB Symp. on Two-topics in X-Ray Astronomy*. ESA SP-296, p. 783
- Johnson W. N. et al., 1994, in Fichtel C. E., Gehrels N., Noms J. P., eds, *The Second Compton Symposium*. IAP, New York, p. 515
- Lahav O. et al., 1993, *Nat*, 364, 693
- Lightman A. P., White T. R., 1988, *ApJ*, 335, 57
- Lightman A. P., Zdziarski A. A., 1987, *ApJ*, 319, 643

L60 *A. A. Zdziarski et al.*

- Madejski G. M. et al., 1994, ApJ, in press (M94)  
Maisack M. et al., 1993, ApJ, 407, L61  
Nandra K., Pounds K., 1994, MNRAS, 268, 405 (NP94)  
Piccinotti G., Mushotzky R. F., Boldt E. A., Holt S. S., Marshall F. E., Serlemitsos P. J., Shafer R. A., 1982, ApJ, 253, 485  
Piro L., Yamauchi M., Matsuoka M., 1990, ApJ, 360, L35  
Pounds K. A., Nandra K., Stewart G. C., George I. M., Fabian A. C., 1990, Nat, 344, 132  
Pozdnyakov I. A., Sobol' I. M., Sunyaev R. A., 1977, AZh, 54, 1246 (English translation in Sov. Astron.-AJ, 21, 708)  
Press W. H., Teukolsky S. A., Vetterling W. T., Flannery B. P., 1992, Numerical Recipes, 2nd edn. Cambridge Univ. Press, Cambridge  
Rothschild R. E., Mushotzky R. F., Baity W. A., Gruber D. E., Matteson J. L., Peterson L. E., 1983, ApJ, 269, 423  
Sunyaev R. A., Titarchuk L. G., 1980, A&A, 86, 121  
Svensson R., 1984, MNRAS, 209, 175  
Svensson R., 1987, MNRAS, 227, 403 (S87)  
Svensson R., Zdziarski A. A., 1994, ApJ, in press  
Trombka J. I., Dyer C. S., Evans L. G., Bielefeld M. J., Seltzer S. M., Metzger A. E., 1977, ApJ, 212, 925  
White T. R., Lightman A. P., Zdziarski A. A., 1988, ApJ, 331, 939  
Zdziarski A. A., 1985, ApJ, 289, 514 (Z85)  
Zdziarski A. A., 1986, ApJ, 303, 94  
Zdziarski A. A., Lightman A. P., Maciołek-Niedźwiecki A., 1993, ApJ, 414, L93